Supporting Information for "The influence of Southern Ocean surface buoyancy forcing on glacial-interglacial changes in the global deep ocean stratification"

Shantong Sun,[1] Ian Eisenman,[1] and Andrew L. Stewart [2]

[1] Scripps Institution of Oceanography, University of California, San Diego, La Jolla, USA
[2] Department of Atmospheric and Oceanic Sciences, University of California, Los Angeles, USA

Contents of this file

1. Text S1 to S3
2. Table S1
3. Figures S1 to S10

Introduction

This Supporting Information comprises three sections of text, one table, and ten figures. In Text S1, the CESM simulation set-up is described in detail. In Text S2, we present further analysis of the deep ocean stratification and discuss the issue of model equilibration. In Text S3, we derive the conceptual model used in the main text.

Text S1. CESM setup

We run CESM version 1.1.2 using a configuration in which only the ocean is active. The ocean component of CESM is the Parallel Ocean Program version 2 (POP2) [*Danabasoglu et al.*, 2012], which has 60 vertical levels ranging from 10m at the surface to 250m at the ocean bottom. We use the CESM "f09_g16" grid, which has a horizontal resolution of nominally 1° with the north pole of the ocean grid displaced to Greenland. This is the same grid configuration that was used in the coupled PI simulation [*Gent et al.*, 2011] and the coupled LGM simulations [*Brady et al.*, 2013], from which the forcing in this study is derived. The coupled simulations have a resolution for the land and atmosphere components of $1.9° \times 2.5°$ and the same resolution for the sea ice component as for the ocean.

The Gent-McWilliams (GM) parameterization [*Gent and Mcwilliams*, 1990] is used to represent the unresolved mesoscale eddies. A GM coefficient is adopted that varies proportional to the local density stratification. This coefficient varies in the horizontal directions and decays with depth, mimicking the decay of eddy activity with depth [*Gent and Danabasoglu*, 2011; *Gent*, 2016]. This allows the model simulations to compare more favorably with observations than models that use a constant diffusivity [*Danabasoglu and Marshall*, 2007], and it enables the model to simulate a response to perturbations in the surface forcing that is comparable to simulations run at much higher resolutions [*Gent and Danabasoglu*, 2011; *Gent*, 2016].

The forcing for each ocean-only simulation is constructed from the coupled model output as a series of repeating 30-year cycles using simulations years 1050-1079 of the coupled PI simulation and 1870-1899 of the coupled LGM simulation. Atmospheric forcings including precipitation, solar radiation, surface winds speed, atmospheric pressure, and atmospheric humidity are taken from output reported by the CCSM4 coupler and have 3-hr temporal resolution. Fluxes across the atmosphere-ocean interface, including evaporation, wind stress, upward longwave radiation, latent heat flux, and sensible heat flux, are calculated in the ocean-only runs based on the simulated ocean state and the specified atmospheric state. For ice-related forcing including sea ice concentration (i.e., fraction of grid box covered by ice) and heat flux between the ice and the ocean, we use daily-mean

Corresponding author: Shantong Sun, shantong@ucsd.edu

data reported by the CCSM4 sea ice component (CICE). For other ice-related forcing including freshwater flux, ice/ocean stress, and salt flux, daily output is not available so we use monthly-mean data reported by CICE. For river runoff and glacial runoff we used monthly-mean data reported by the CCSM4 land component (CLM4).

In order to obtain better agreement between the coupled runs and the ocean-only runs, a process called "diddling" is performed on all monthly-mean data. This allows the monthly-mean values to be preserved when the model linearly interpolates between values at the midpoint of each month. Details are given in *Killworth* [1996].

The sea level was about 100m lower at the LGM than today due to the presence of larger high-latitude ice sheets. This gives rise to slightly different coastlines at the LGM, which is accounted for in the coupled CCSM4 LGM simulation. In order to isolate the influence of surface forcing alone, in the present study we use modern ocean bathymetry in the LGM and Test simulations, as in the PI simulation. As a result, some ocean regions in the ocean-only simulations are land in the coupled LGM simulation that is used to generate the forcing fields. If these areas are not treated appropriately, they can lead to the generation of extremely cold surface water due to the direct contact with the cold terrestrial atmosphere in locations where sea ice would have formed if the sea ice model were active (this is exacerbated by the fact that the surface air in some of these locations is hundreds of meters above the sea level at the surface of the ice sheet in the coupled LGM simulation). To address this issue, both the sea ice concentration and atmospheric forcing need to be adjusted when we apply LGM forcing in locations that are ocean in the PI bathymetry but land in the coupled LGM simulation. We adjust the surface air temperature and potential temperature in these locations by assuming a constant lapse rate of $-6.5^{\circ}\mathrm{C}/\mathrm{km}$ to account for the change of surface geopotential height between the coupled LGM and coupled PI runs. The surface atmospheric pressure is adjusted by assuming exponential decay with height, $p = p_0 \exp(-z/H)$, where $H = 7.6$km is the scale height. The sea ice concentration (c) in these grid cells is prescribed based on the surface air temperature (T) as $c = 1/2 \tanh[(T - T_0)/T_0] + 1/2$, where $T_0 = -2^{\circ}$C. This is motivated by the observation that in the coupled simulations, most ocean locations with surface air temperature below -5°C have ice concentrations close to 100%, and most ocean locations with surface air temperature above 0°C have ice concentrations close to 0%. All fluxes between the ice and ocean in these grid cells are set to zero, including the freshwater flux, salt flux, and momentum flux.

All forcing fields in the ocean-only simulations are from the coupled simulations as specified in Section 2 of the main text, with two exceptions. First, all three ocean-only simulations use the same run-off forcing, which is derived from the coupled PI run. Second, for the weak restoring of surface salinity, which is included in the ocean-only model as described in *Griffies et al.* [2009], the Test run uses salinity restoring field derived from the coupled PI run at all locations, including the Southern Ocean. This simplification appears to have only a small influence on the Test run: the difference between the LGM and Test freshwater fluxes associated with the weak restoring of surface salinity in most Southern Ocean locations is less than 10% of the difference between the LGM and PI runs (not shown), and the surface buoyancy forcing profiles in the Southern Ocean are nearly indistinguishable between the LGM and Test runs (see Figure 1 in the main text).

The surface temperature and salinity for the three ocean-only runs are shown in Figs. S1 and S2. In general, the surface salinity is less constrained by the forcing than the surface temperature. This is expected because the freshwater flux more closely resembles a fixed flux, while the heat flux more closely resembles a relaxation boundary condition [*Haney*, 1971] that tends to fix the surface temperature. Under fixed flux boundary conditions, the actual value of surface salinity is strongly influenced by salt fluxes within the ocean.

Text S2. Details of the deep ocean stratification and model equilibration

The zonal mean stratification in the Atlantic Ocean is shown in Figure S3, with the basin-average stratification profile given in Figure S4 for the South Atlantic, South Pacific, and Indian

Table S1. Durations of model simulations and trends of global volume-average temperature, ideal age, and AMOC max calculated over the last 120 years of each run.

Run Name	PI	Test	LGM
Surface forcing	PI	PI&LGM	LGM
Duration (years)	510	1020	1440
Temperature trend ($^\circ$C/century)	-0.046	-0.048	-0.053
Ideal Age trend (year/century)	16.8	8.8	9.6
AMOC max trend (Sv/Century)	-0.28	-0.16	-0.64

Oceans, and in Figure S5 for the North Atlantic, North Pacific, and Southern Oceans. In every ocean basin the Test run approximately reproduces the LGM deep ocean stratification below 2000m. The deep stratification in the Atlantic Ocean is stronger than in the other ocean basins, which is likely due to the presence of the North Atlantic Deep Water (NADW).

Figure S6 shows the change in the stratification between the last two 30-year periods in the Atlantic Ocean as an indication of the level of equilibration in the simulations. The PI run has a similar trend to the Test run, while the LGM run has a trend that is approximately 3 times larger. The magnitude of the deep ocean stratification changes from one 30-year period to the next (Figure S6) are approximately 100 times smaller than the differences between the three simulations (Figure S3).

Text S3. Conceptual model

S3.i: Derivation of the conceptual model

The derivation of the conceptual model follows *Nikurashin and Vallis* [2011] and *Nikurashin and Vallis* [2012]; see these studies for further details. The model takes a zonally-averaged view of the global stratification and overturning circulation, which are described by the zonal-mean buoyancy $b^* \equiv -g(\rho - \rho_0)/\rho_0$ and overturning circulation streamfunction $\psi(y, z)$. Here we use ψ to describe the zonally integrated circulation rather than the zonal-mean circulation, i.e., ψ has units of m^3/s rather than m^2/s as in *Nikurashin and Vallis* [2012]. The ocean is approximated to consist of a single basin (e.g., the Atlantic) of meridional length L_y and zonal length L_x, which is connected to a re-entrant zonal channel at the southern boundary (resembling the Southern Ocean). This configuration is sketched in Figure 2c in the main text. In the basin the isopycnals are assumed to be flat, so we define $b(z) \equiv b^*(y, z)$ for all $y > 0$, while in the channel ($y < 0$) the isopycnals are assumed to have a constant isopycnal slope s. The surface of the channel is subject to a fixed downward buoyancy flux $B(y)$, and the formation of NADW at the northern end of the basin is represented by $\psi^*(z) \equiv \psi(L_y, z)$. The flow in the channel is assumed to be adiabatic, while the basin is subject to a constant diapycnal diffusivity κ.

Following *Nikurashin and Vallis* [2012], volume conservation implies that at a given depth, the change in the overturning streamfunction across the basin is equal to the net upwelling driven by diapycnal diffusion within the basin,

$$\psi^*(z) - \psi(0, z) = \frac{\kappa\, L_y\, L_x}{N^2} \frac{\partial}{\partial z} N^2(z), \tag{S1}$$

where $y = 0$ represents the northern boundary of the Southern Ocean (Figure 2c). Here $N^2 \equiv \partial b/\partial z$ is the Brunt-Väisälä frequency, which is a measure of the ocean density stratification. For isopycnals that outcrop in the Southern Ocean, the overturning streamfunction at the base of the

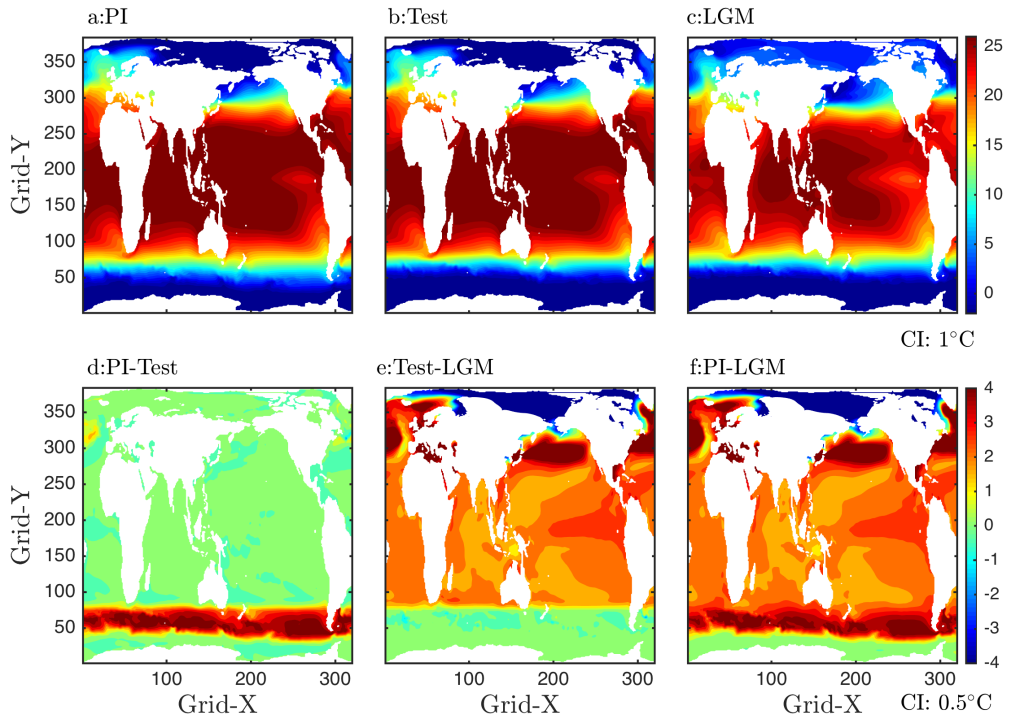

Figure S1. Long-term mean surface potential temperature (° C) in the three model runs and the differences between them. The fields are plotted here on the coordinates of the ocean model grid, which has the North Pole displaced to Greenland [*Danabasoglu et al.*, 2006].

mixed layer ($z = 0$) can be related to the surface buoyancy forcing by

$$\psi(y, 0) = \frac{L_x\, B(y)}{\partial b/\partial y} \tag{S2}$$

for $y < 0$ [cf. *Marshall and Radko*, 2003]. Since the overturning circulation is assumed to be adiabatic in the Southern Ocean, the value of the streamfunction at the base of the mixed layer ($z = 0$) must match the value at the northern edge of the channel ($y = 0$) along the same isopycnal. For constant isopycnal slope s in the Southern Ocean, this implies

$$\psi(-z/s, 0) = \psi(0, z). \tag{S3}$$

Combining equation (S1), (S2), and (S3), we obtain

$$\frac{\kappa\, L_y\, L_x}{N^2(z)} \frac{\partial}{\partial z} N^2(z) = \psi^*(z) + L_x \frac{B(-z/s)}{s\, N^2(z)}, \tag{S4}$$

which is equivalent to equation (2) in the main text.

Isopycnals in Region 3 outcrop only in the Southern Ocean, and ψ^* is zero at the northern boundary. Therefore equation (S4) reduces to

$$\kappa\, s\, L_y \frac{\partial}{\partial z} N^2(z) = B(-z/s), \tag{S5}$$

which is equivalent to equation (3) in the main text. Assuming that N^2 is negligibly small at the bottom boundary $z = z_{bot}$ (see Figure 3a in the main text), integration of equation (S5) shows that

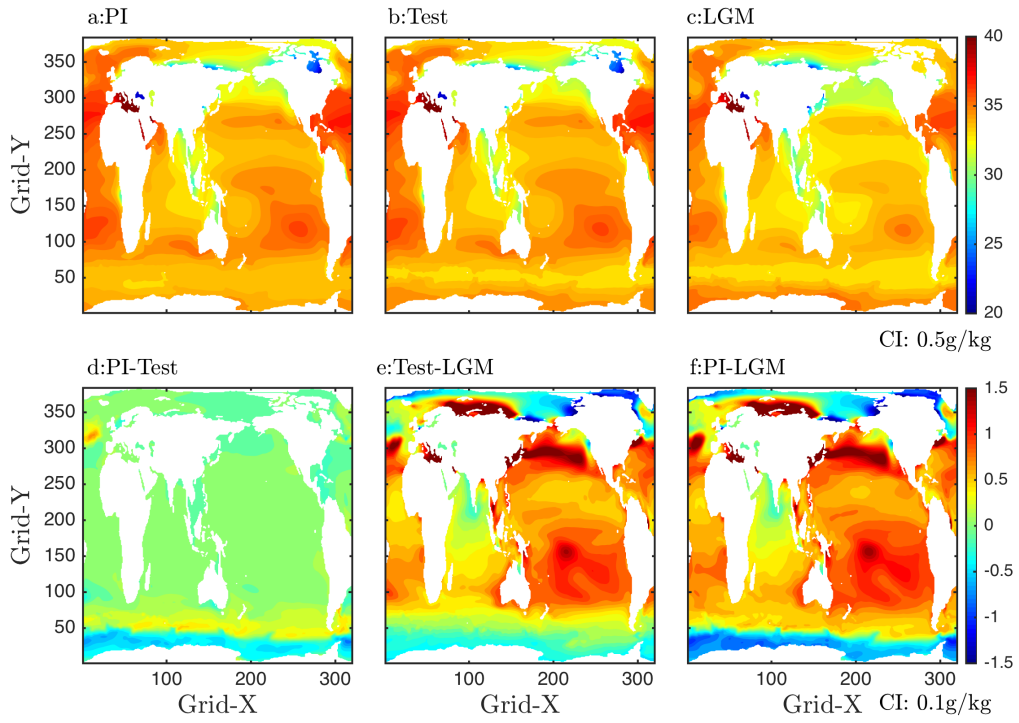

Figure S2. Long-term mean surface salinity (g/kg) in the three model runs and the differences between them. Coordinates are as in Figure S1.

the stratification in Region 3 is determined by the surface buoyancy forcing in the Southern Ocean only as long as B is specified:

$$N^2(z) = \int_{z_{bot}}^{z} \frac{B(-z'/s)}{\kappa\, s\, L_y} dz'. \tag{S6}$$

However, if the surface buoyancy forcing takes the form of a relaxation boundary condition, $B(y) = r\,[\,b_s(y) - b^*(y,0)\,]$ with r the relaxation coefficient, b_s the specified surface buoyancy, and $b^*(y,0)$ the buoyancy at the surface of the Southern Ocean, then the buoyancy $b(z)$ appears on both sides of equation (S6), so this equation no longer directly indicates what determines the stratification. In this case, equation (S5) becomes

$$\kappa\, s\, L_y \frac{\partial}{\partial z} N^2(z) + r\, b(z) = r\, b_s(-z/s), \tag{S7}$$

where we have used $b^*(y,0) = b^*(-z/s,0) = b(z)$, i.e., the buoyancy in the basin is equal to the buoyancy at the surface of the Southern Ocean along the same isopycnal. Since $N^2 \equiv \partial b/\partial z$, equation (S7) is a second-order ordinary differential equation for $b(z)$. In this case, the abyssal stratification is affected by the upper boundary condition for b, and so it is subject to at least slight inter-hemispheric influences as expected from *Fučkar and Vallis* [2007].

In Region 2, where ψ^* does not vanish, we consider the difference between the stratifications in the LGM and Test runs, which can be derived from equation (S4) as

$$\kappa\, L_y\, L_x \frac{\partial}{\partial z}\left(N^2_{\mathrm{LGM}}(z) - N^2_{\mathrm{Test}}(z)\right) = \left(N^2_{\mathrm{LGM}}(z)\psi^*_{\mathrm{LGM}}(z) - N^2_{\mathrm{Test}}(z)\psi^*_{\mathrm{Test}}(z)\right) + \frac{L_x}{s}\left(B_{\mathrm{LGM}}(-z/s) - B_{\mathrm{Test}}(-z/s)\right), \tag{S8}$$

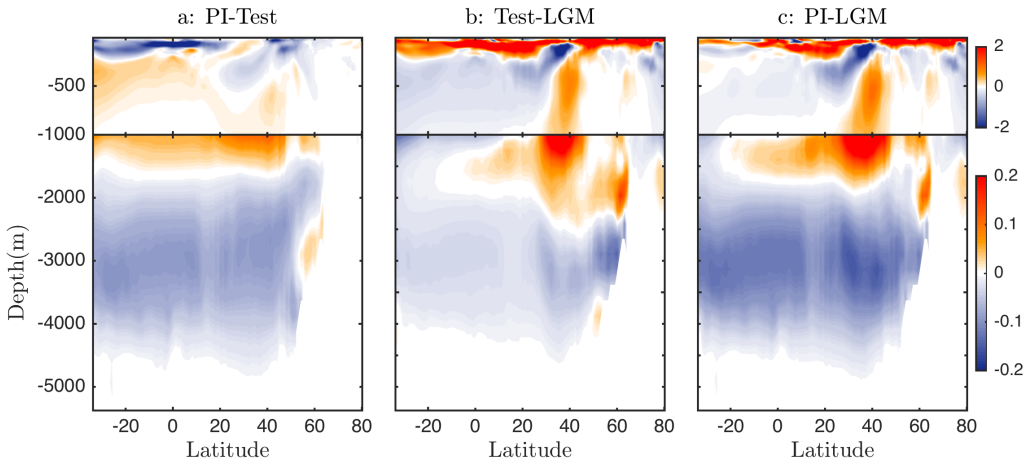

Figure S3. Comparison of the zonal-mean stratification in the Atlantic Ocean between the three model runs (N^2, in units of 10^{-5} s^{-2}). Note that the magnitude of the stratification difference in panel b below about 2000m is 10 times smaller than that in panels a and c.

where the subscripts indicate the simulation name. Since both the LGM and Test simulations are subject to the same approximately fixed LGM surface forcing in the Southern Ocean, we approximate the last term in equation (S8) to be negligibly small (see Figure 1 in the main text), and equation (S8) becomes

$$\begin{aligned}
\kappa\, L_y L_x \frac{\partial}{\partial z}\left(N^2_{\rm LGM}(z) - N^2_{\rm Test}(z)\right) &= N^2_{\rm LGM}(z)\psi^*_{\rm LGM}(z) - N^2_{\rm Test}(z)\psi^*_{\rm Test}(z) \\
&= N^2_{\rm LGM}(z)\left(\psi^*_{\rm LGM}(z) - \psi^*_{\rm Test}(z)\right) + \\
&\qquad \psi^*_{\rm Test}(z)\left(N^2_{\rm LGM}(z) - N^2_{\rm Test}(z)\right) \\
&= N^2_{\rm LGM}(z)\Delta\psi^* + \psi^*_{\rm Test}\Delta N^2 \\
&= N^2_{\rm LGM}(z)\Delta\psi^*\left(1 + \frac{\psi^*_{\rm Test}\Delta N^2}{\Delta\psi^* N^2}\right). \qquad \text{(S9)}
\end{aligned}$$

At the depth of isopycnal surface ρ_2 that separates the upper and lower overturning cells, defined here as z_0, $N^2_{\rm LGM} \approx N^2_{\rm Test} \gg \Delta N^2$ and $\psi^*_{\rm Test} \sim \psi^*_{\rm LGM} \sim \Delta\psi^* \sim 0$, as discussed above. Hence $\frac{\psi^*_{\rm Test}\Delta N^2}{\Delta\psi^* N^2} \ll 1$ and equation (S9) can be approximately written near $z = z_0$ as

$$\kappa\, L_y\, L_x \frac{\partial}{\partial z}\Delta N^2(z) \approx N^2_{\rm LGM}(z)\Delta\psi^*(z), \qquad \text{(S10)}$$

where $\Delta N^2 \equiv N^2_{\rm LGM} - N^2_{\rm Test}$ and $\Delta\psi^* \equiv \psi^*_{\rm LGM} - \psi^*_{\rm Test}$. Using a realistic Atlantic area of $L_x\, L_y = 8 \times 10^{13}$m^2, diapycnal diffusivity of $\kappa = 1 \times 10^{-4}$ m^2/s, and Region 2 approximate depth range of $\delta z = 1000$m, this implies that the NADW streamfunction must differ between the LGM and Test runs by $\Delta\psi^* \approx 8\,$Sv in order to produce an order-one fractional change in the vertical change of the stratification over the depth of Region 2. Given the small change in NADW of about 2 Sv between the LGM and Test simulations, we suggest that this explains why the change in stratification across the depth range of Region 2 (approximately 2km to 3km) is similar in the LGM and Test simulations (red and green lines in Figure 3a of the main text).

Note that in Region 1, the influence from the surface wind-driven circulation is non-negligible, so the assumption adopted here of flat isopycnals in the basin is not applicable.

An important caveat is that this conceptual model is only used in order to achieve a qualitative understanding of the influence of the Southern Ocean surface forcing on the abyssal and mid-depth

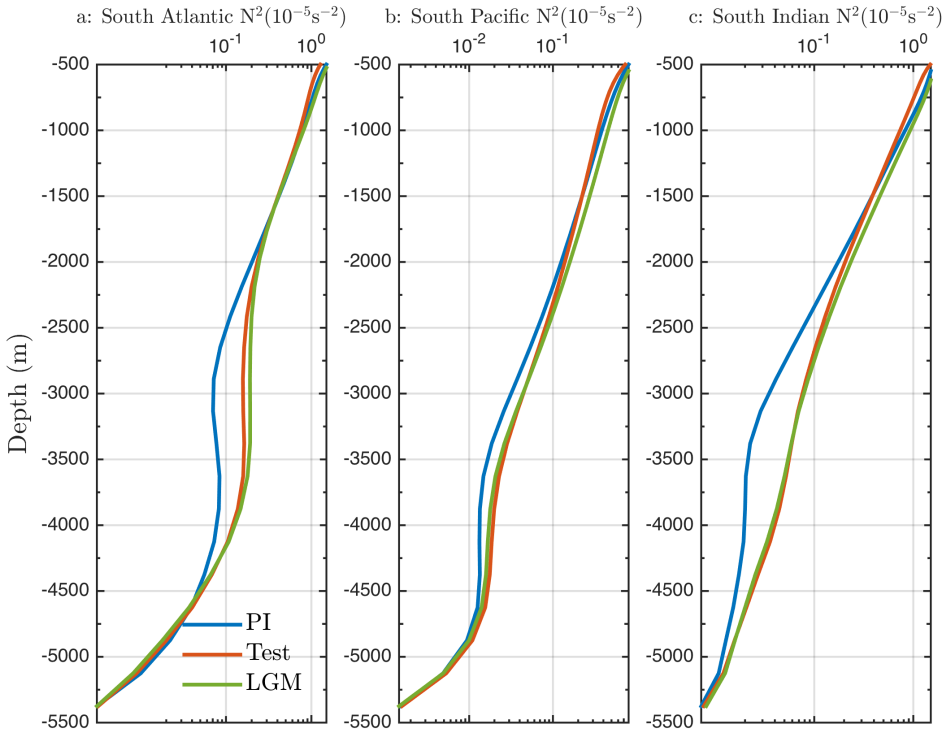

Figure S4. Basin-averaged stratification in the South Atlantic, South Pacific, and South Indian Oceans (N^2, in units of 10^{-5} s^{-2}).

stratification. This model should not be expected to quantitatively reproduce the stratification profiles shown in Figure S4 and S5. For example, the stratification in the Atlantic is clearly different from the other basins, which is not accounted for in this conceptual model. Furthermore, the assumption of an adiabatic Southern Ocean circulation in our conceptual model is not strictly justified. This can be seen in Figure S7, which shows the residual overturning circulation streamfunction in the Southern Ocean for the three model runs, calculated in σ_2 coordinates. A diabatic component to the circulation south of 50°S is readily discernible. This enhanced diapycnal flow in the Southern Ocean is mainly associated with the deep mixed layer inside the subpolar gyre. Away from the subpolar gyre region, the residual overturning circulation streamfunction approximately follows isopycnals, i.e., the adiabatic assumption is approximately satisfied.

S3.ii: Non-constant isopycnal slope

In the analysis above, we assumed a constant isopycnal slope in the Southern Ocean for simplicity, and we concluded that the NADW streamfunction would need to differ considerably between the LGM and Test runs to produce a substantial change in the stratification of Region 2. Here we show this conclusion still holds if we relax the assumption of constant isopycnal slope in the Southern Ocean to allow the slope to vary between different isopycnals. Note that this analysis will focus on the Southern Ocean region, whereas the analysis in Section S3.i focused on the basin north of the Southern Ocean.

Following *Nikurashin and Vallis* [2011], the residual overturning circulation streamfunction in the Southern Ocean can be written as

$$\psi = \psi^{+} + \psi^{\#}. \tag{S11}$$

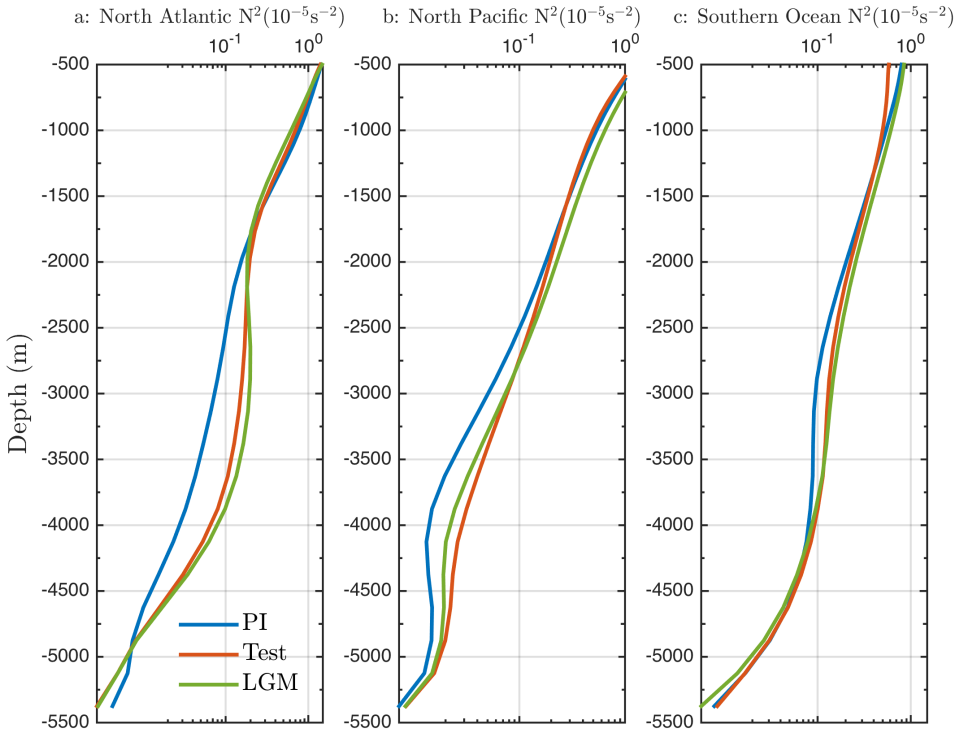

Figure S5. Basin-averaged stratification in the North Atlantic, North Pacific, and Southern Oceans (N^2, in units of 10^{-5} s^{-2}).

Here, ψ^+ represents the contribution from mean flow and is given by the surface Ekman transport,

$$\psi^+ = -\frac{\tau_0 \, L_x}{f_0 \rho_0}, \tag{S12}$$

and $\psi^\#$ is the eddy-driven overturning circulation streamfunction which can be expressed as

$$\psi^\# = L_x \, K_{\rm GM} \, s \tag{S13}$$

based on the Gent-McWilliams (GM) parameterization of mesoscale eddies. Here $K_{\rm GM}$ is the GM thickness diffusivity which is a function of the local stratification in our ocean-only CESM simulations. We assume for simplicity that the surface wind stress forcing (τ_0) and Coriolis parameter (f_0) are constant, which implies that ψ^+ is constant across the Southern Ocean and all Eulerian-mean vertical motions occur in the southern and northern boundary of the Southern Ocean. This simplification is also made in *Nikurashin and Vallis* [2011] for qualitative discussions.

In the ocean-only CESM simulations, both the GM thickness diffusivity $K_{\rm GM}$ and isopycnal slope s vary somewhat in the Southern Ocean (Figure S9 and S10), and they combine together to support the southward NADW transport into the Southern Ocean as in *Abernathey et al.* [2011], i.e., both $K_{\rm GM}$ and s vary to account for the vertical change of ψ at the northern boundary of the Southern Ocean. Here, for simplicity, we only allow s to vary but keep $K_{\rm GM}$ constant, as in previous idealized modeling studies [e.g., *Wolfe and Cessi*, 2011].

Furthermore, we assume the circulation in the Southern Ocean to be adiabatic, i.e., the residual overturning circulation streamfunction ψ is constant along each individual isopycnal surface. Hence the assumption of a constant ψ^+ implies that the eddy-driven overturning circulation streamfunction $\psi^\#$ must also be constant along each isopycnal surface.

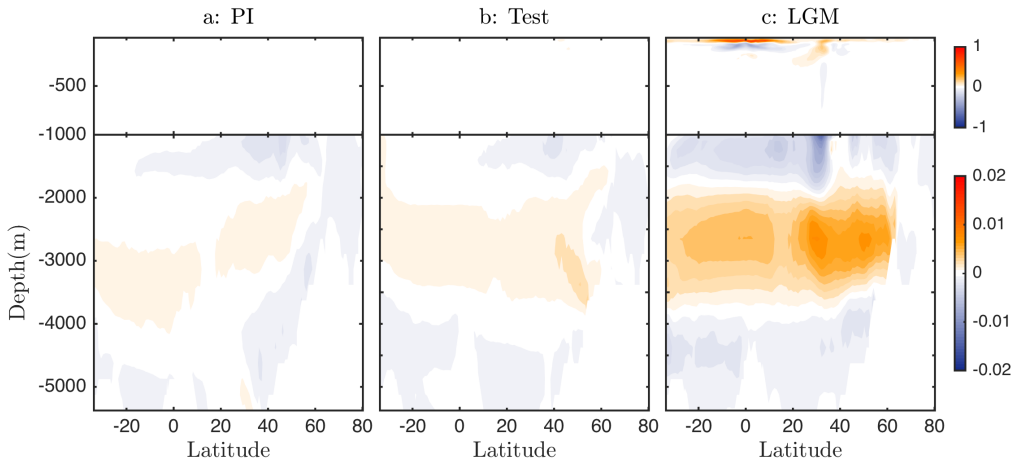

Figure S6. Change of the zonal-mean stratification in the Atlantic Ocean between the last two 30-year cycles (N^2, in units of 10^{-5} s^{-2}). Note that the magnitude of the stratification change in the deep ocean is of order 0.001×10^{-5} s^{-2}, which is 100 times smaller than in Figure S3.

Consider the residual overturning circulation on two isopycnals, ρ_2 and ρ_*, where ρ_2 is indicated in Figure 2c as the isopycnal that separates the abyssal overturning circulation from the region above, and ρ_* can be any isopycnal between ρ_1 and ρ_2. In the Southern Ocean, the southward flux of NADW ($\psi_{\rm NADW}$) between ρ_2 and ρ_* has to be balanced by the vertical change in the eddy-driven overturning circulation streamfunction since the Eulerian-mean overturning circulation (ψ^+) has been assumed to be constant,

$$\psi_{\rm NADW} = \psi_* - \psi_2 = \psi_*^{\#} - \psi_2^{\#}. \tag{S14}$$

Here, ψ_* and ψ_2 are the residual overturning circulation streamfunction on isopycnal surface ρ_* and ρ_2, and $\psi_*^{\#}$ and $\psi_2^{\#}$ are the eddy-driven overturning circulation streamfunction on isopycnal surfaces ρ_* and ρ_2. Combining equation (S13) and (S14), we have

$$\psi_{\rm NADW} = L_x K_{\rm GM}(s_* - s_2), \tag{S15}$$

where s_* and s_2 are the slopes of isopycnals ρ_* and ρ_2, respectively. At the surface of the Southern Ocean, the upwelled water is transformed to lighter water by the surface buoyancy flux B (which is fixed, i.e., independent of the ocean state), which satisfies

$$\frac{B}{\partial b/\partial y} = \frac{\psi_{\rm NADW}}{L_x}. \tag{S16}$$

In equation (S16), both B and $\partial b/\partial y$ are evaluated at the surface in the Southern Ocean where ρ_* outcrops. The buoyancy gradient $\partial b/\partial y$ can be approximated by

$$\frac{\partial b}{\partial y} \approx -\frac{\rho_* - \rho_2 g}{\rho_0 W} = \frac{g'}{W}, \tag{S17}$$

where $g' \equiv (\rho_* - \rho_2 g)/\rho_0$ and W is the distance between ρ_2 and ρ_* at the ocean surface, i.e.,

$$W = \frac{z_2}{s_2} - \frac{z_*}{s_*}. \tag{S18}$$

Based on our definition of ρ_2,

$$\psi_2 = 0 \text{ and } \mathrm{s_2} = -\frac{\tau_0}{\rho_0 \mathrm{f_0 K_{GM}}} \tag{S19}$$

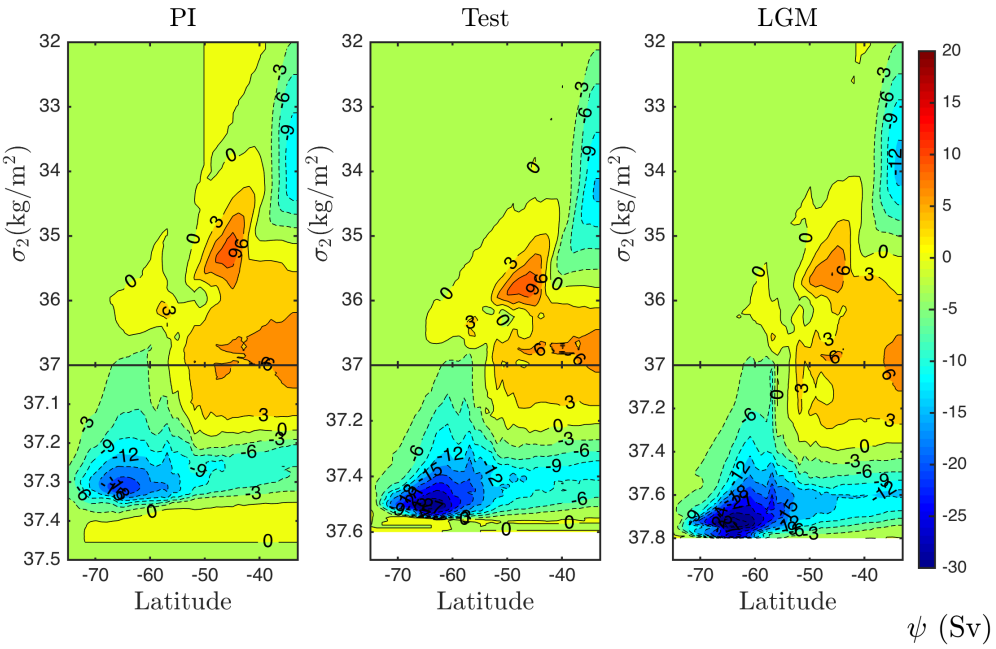

Figure S7. Residual overturning circulation streamfunction in the Southern Ocean (Sv) using σ_2 as the vertical coordinate.

are specified constants.

Combining equation (S16), (S17) and (S18), we obtain

$$\frac{B}{g'}\left(\frac{z_2}{s_2}-\frac{z_*}{s_*}\right)=\frac{\psi_{\mathrm{NADW}}}{L_x}. \tag{S20}$$

Substituting equation (S15) into (S20) leads to

$$\frac{B}{g'}\left[\frac{z_2}{s_2}-\frac{z_*}{s_2+\psi_{\mathrm{NADW}}/(K_{\mathrm{GM}}L_x)}\right]=\frac{\psi_{\mathrm{NADW}}}{L_x}, \tag{S21}$$

from which we can obtain

$$\frac{z_*}{s_2+\psi_{\mathrm{NADW}}/(K_{\mathrm{GM}}L_x)}=\frac{z_2}{s_2}-\frac{\psi_{\mathrm{NADW}}\,g'}{BL_x}. \tag{S22}$$

Therefore, the difference in depth between ρ_* and ρ_2 is

$$z_*-z_2=\underbrace{\frac{z_2}{s_2}\frac{\psi_{\mathrm{NADW}}}{K_{\mathrm{GM}}L_x}}_{\mathrm{I}}-\underbrace{\frac{\psi_{\mathrm{NADW}}\,g'}{BL_x}\left(s_2+\frac{\psi_{\mathrm{NADW}}}{K_{\mathrm{GM}}L_x}\right)}_{\mathrm{II}}. \tag{S23}$$

Here Term I represents the effect of the reduction in the isopycnal slope that supports a positive overturning overturning streamfunction because $s_*-s_2=\psi_{\mathrm{NADW}}/(L_xK_{\mathrm{GM}})$ from equation (S15). Term II represents the contribution from the northward displacement of the outcropping latitude of ρ_* relative to ρ_2 because $(\psi_{\mathrm{NADW}}\,g')/(BL_x)\approx W$ based on equation (S16) and (S17).

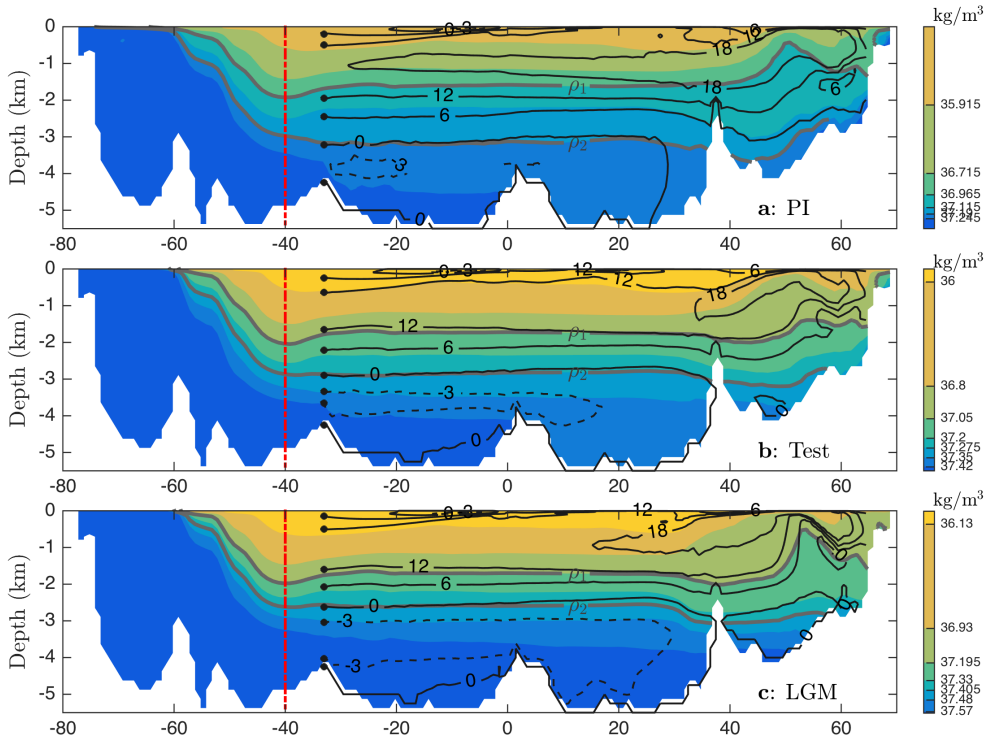

Figure S8. As in Figure 2b in the main text, but including the PI and LGM simulations as well as the Test simulation. (Note that panel b here is equivalent to Figure 2b.)

For typical values in the real ocean:

$$\begin{aligned} \psi_{\mathrm{NADW}} &= 10^7 \mathrm{m}^3/\mathrm{s}, & s_2 &= -10^{-3}, \\ L_x &= 2\times 10^7 \mathrm{m}, & \rho_0 &= 1000 \mathrm{kg/m}^3, \\ K_{\mathrm{GM}} &= 1000 \mathrm{m}^2/\mathrm{s}, & \rho_2 - \rho_* &= 0.2 \mathrm{kg/m}^3, \\ B &= 10^{-8} \mathrm{m}^2/\mathrm{s}^3, & z_2 &= -3000 \mathrm{m}. \end{aligned}$$

Here the value of ρ_* is chosen close to the core of the NADW overturning circulation, where there is maximal change in the isopycnal slope.

We obtain

$$z_* - z_2 = \underbrace{1500m}_{\mathrm{I}} + \underbrace{50m}_{\mathrm{II}}\,. \tag{S24}$$

Clearly, term I dominates over term II in equation (S23). Thus, we have

$$z_* - z_2 \approx \frac{z_2 \psi_{\mathrm{NADW}}}{s_2\, K_{\mathrm{GM}} L_x}. \tag{S25}$$

Inserting equation (S25) into the approximate derivative $N^2 \approx g'/(z_* - z_2)$, the density stratification in Region 2 is

$$N^2 \approx \frac{\Lambda}{\psi_{\mathrm{NADW}}}, \tag{S26}$$

with

$$\Lambda \equiv \frac{g' s_2\, K_{\mathrm{GM}} L_x}{z_2} \tag{S27}$$

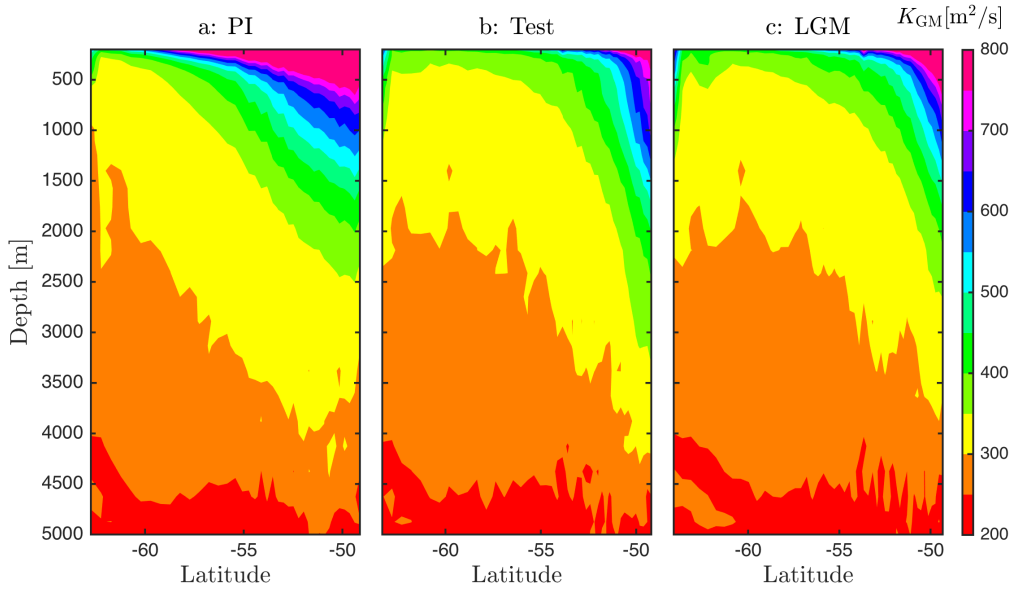

Figure S9. Gent-McWilliams (GM) thickness diffusion coefficient (K_{GM}; units of m^2/s) averaged zonally along barotropic streamlines.

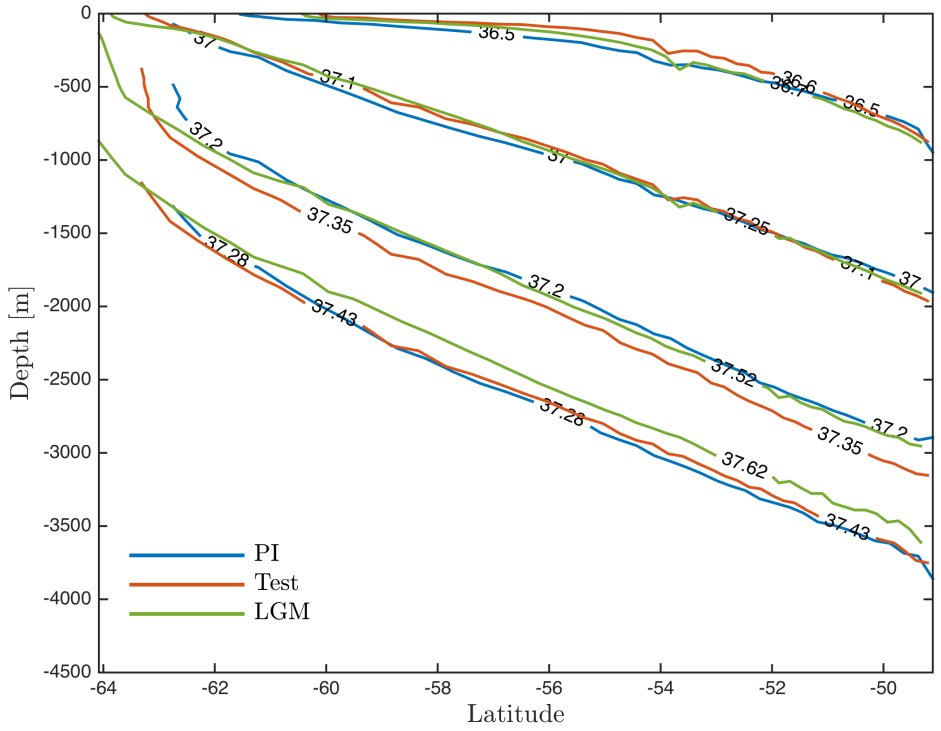

Figure S10. Isopycnal contours of σ_2 (units of kg/m^3) averaged zonally along barotropic streamlines.

being a constant. From equation (S26), we obtain

$$\Delta N^2 \approx -\frac{\Lambda}{\psi^2_{\mathrm{NADW:LGM}}}\Delta\psi_{\mathrm{NADW}}. \tag{S28}$$

Here $\Delta\psi_{\mathrm{NADW}} \equiv \psi_{\mathrm{NADW:LGM}} - \psi_{\mathrm{NADW:Test}}$, where $\psi_{\mathrm{NADW:LGM}}$ and $\psi_{\mathrm{NADW:Test}}$ are the values of ψ_{NADW} in the LGM and Test simulations. Recall that $\Delta N^2 \equiv N^2_{\mathrm{LGM}} - N^2_{\mathrm{Test}}$. To obtain equation (S28), we have used the assumption $\psi_{\mathrm{NADW:LGM}} \approx \psi_{\mathrm{NADW:Test}}$. Combining equation (S26) with (S28) leads to

$$\frac{\Delta N^2}{N^2_{\mathrm{LGM}}} \approx -\frac{\Delta\psi_{\mathrm{NADW}}}{\psi_{\mathrm{NADW:LGM}}}. \tag{S29}$$

Therefore, even when the assumption of constant isopycnal slope is relaxed, an order-one change in NADW transport is still required for the Northern Hemisphere surface forcing alone to cause an order-one change in the density stratification in Region 2. Consistent with the simpler analysis in Section S3.i, we suggest that this explains why the stratification in Region 2 was relatively insensitive to changes in Northern Hemisphere surface forcing.

References

Abernathey, R., J. Marshall, and D. Ferreira (2011), The dependence of Southern Ocean meridional overturning on wind stress, *J. Phys. Oceanogr.*, *41*(12), 2261–2278.

Brady, E. C., B. L. Otto-Bliesner, J. E. Kay, and N. Rosenbloom (2013), Sensitivity to glacial forcing in the CCSM4, *J. Clim.*, *26*(6), 1901–1925.

Danabasoglu, G., and J. Marshall (2007), Effects of vertical variations of thickness diffusivity in an ocean general circulation model, *Ocean Modell.*, *18*(2), 122–141.

Danabasoglu, G., W. G. Large, J. J. Tribbia, P. R. Gent, B. P. Briegleb, and J. C. McWilliams (2006), Diurnal coupling in the tropical oceans of CCSM3, *J. of Clim.*, *19*(11), 2347–2365.

Danabasoglu, G., S. C. Bates, B. P. Briegleb, S. R. Jayne, M. Jochum, W. G. Large, S. Peacock, and S. G. Yeager (2012), The CCSM4 ocean component, *J. Clim.*, *25*(5), 1361–1389.

Fučkar, N. S., and G. K. Vallis (2007), Interhemispheric influence of surface buoyancy conditions on a circumpolar current, *Geophys. Res. Lett.*, *34*(14).

Gent, P. R. (2016), Effects of Southern Hemisphere Wind Changes on the Meridional Overturning Circulation in Ocean Models, *Annu. Rev. Mar. Sci.*, *8*, 79–84.

Gent, P. R., and G. Danabasoglu (2011), Response to increasing Southern Hemisphere winds in CCSM4, *J. Clim.*, *24*(19), 4992–4998.

Gent, P. R., and J. C. Mcwilliams (1990), Isopycnal mixing in ocean circulation models, *J. Phys. Oceanogr.*, *20*(1), 150–155.

Gent, P. R., G. Danabasoglu, L. J. Donner, M. M. Holland, E. C. Hunke, S. R. Jayne, D. M. Lawrence, R. B. Neale, P. J. Rasch, M. Vertenstein, et al. (2011), The community climate system model version 4, *J. Clim.*, *24*(19), 4973–4991.

Griffies, S. M., A. Biastoch, C. Böning, F. Bryan, G. Danabasoglu, E. P. Chassignet, M. H. England, R. Gerdes, H. Haak, R. W. Hallberg, et al. (2009), Coordinated ocean-ice reference experiments (COREs), *Ocean Modell.*, *26*(1), 1–46.

Haney, R. L. (1971), Surface thermal boundary condition for ocean circulation models, *J. Phys. Oceanogr.*, *1*(4), 241–248.

Killworth, P. D. (1996), Time interpolation of forcing fields in ocean models, *J. Phys. Oceanogr.*, *26*(1), 136–143.

Marshall, J., and T. Radko (2003), Residual-mean solutions for the Antarctic Circumpolar Current and its associated overturning circulation, *J. Phys. Oceanogr.*, *33*(11), 2341–2354.

Nikurashin, M., and G. Vallis (2011), A theory of deep stratification and overturning circulation in the ocean, *J. Phys. Oceanogr.*, *41*(3), 485–502.

Nikurashin, M., and G. Vallis (2012), A theory of the interhemispheric meridional overturning circulation and associated stratification, *J. Phys. Oceanogr.*, *42*(10), 1652–1667.

Wolfe, C. L., and P. Cessi (2011), The adiabatic pole-to-pole overturning circulation, *J. Phys. Oceanogr.*, *41*(9), 1795–1810.